STUDY OF FLOW AND HEAT TRANSFER FOR PULSATING FILM COOLING BY DYNAMIC MODAL DECOMPOSITION

WANG Wei[1,2], WANG Yu-qing[2], ZHU Nan[1,*], Li Fajing[3]

1.State key Laboratory for Manufacturing System Engineering, Xi'an Jiaotong University, Xi'an 710049, China;

2. National Demonstration Center for Experimental Mechanics Education, College of Mechanical and Vehicle Engineering,Taiyuan University of Technology, Taiyuan, 030024, China

3.Joint Laboratory of Energy Saving and Intelligent Maintainence for Modern Transportations, Guangzhou 510430, China

* Corresponding author; E-mail: nan.zhu@xjtu.edu.cn

The effect of pulsating jet on the unsteady film cooling performance was studied by experimental and numerical simulation. The FLIR thermal infrared thermal camera was used the measure the adiabatic temperature of the surface. The Large Eddy Simulation was conducted for analyzing the adiabatic film cooling effectiveness at four different jet nondimensionalized pulsated frequency of St=0, 0.1, 0.2, and 0.3. The DMD dynamic mode analysis of both the velocity and temperature fields obtained by numerical calculation was performed to obtain the coupling relationship between the flow and heat transfer. Results show that the cooling effectiveness of steady film cooling (St=0) decreases with the increase of blowing ratio. At low blowing ratio (M=0.65), the cooling efficiency of the pulsating jet is significantly lower than the steady-state jet. At the blowing ratio of 1.0 and 1.5, the cooling efficiency of the low frequency pulsating jet (St=0.1) is a little higher than the steady state jet, indicating that the low frequency pulsation under the high blowing ratio can improve the coverage of the cooling air. At high pulsating frequency (St=0.3), the cooling effectiveness is obviously declined.

***Key words**: Turbine blade; Film cooling; pulsating jet; LES; Dynamic mode decomposition*

1 Introduction

With the development of aero-engine, the initial temperature of turbine has gradually increased even up to 2000K, which has far exceeded the supporting temperature of turbine blade materials. Consequently, the thermal design including cooling techniques for airfoils is necessary. Film cooling[1] is one of the most effective cooling methods, in which the cooling air flows out through plenty of angled holes on the airfoil surface and then covers on the surface to protect airfoil from high temperature mainstream. The film cooling can be considered as a jet in cross-flow (JICF) as perspective of fluid mechanics. Studies show that complex large-scale vortex structures will be formed as the jet mixing with the main gas flow[2-4], such as reverse rotating vortex pair, hairpin vortex, horseshoe vortex and jet shear layer vortex. These unsteady vortex structures lead to momentum and heat transfer between the mainstream and the jet, which will affect the film cooling performance and cause the increase of aerodynamic losses, as well. Studying these vortex structures will be critical for obtaining higher film cooling performance in turbine design and optimization.

Actually in real film cooling for gas turbine, the cooling air extracted from the rotating mechanical compressor is always unsteady pulsating flow. This will result in the pulsating film cooling which shows different characteristics from the steady-state jet and needs further consideration,

consequently. The existence of pulsation in compressor injection air highlights the importance of pulsating flow analysis on a complete turbine blade[5]. Moreover, pulsed film cooling can be used to optimize thermal performance[6]. Early in 1995, Bons[7] has studied the effect of pulse frequency on film cooling efficiency with the frequency range of St=0.0059~0.0240. It is concluded that when the blowing ratio BR<1, the steady-state jet has higher cooling efficiency, while as BR>1 the pulsating jet has higher cooling effectiveness on the contrary. Sultan[8] investigated the sinusoidal pulsating film cooling with nondimensionalized frequency of $St=f\cdot d/U$=0, 0.2, 0.3, and 0.5. They concluded that the pulsations has lower cooling efficiency compared with the steady jet. Coulthard[9] experimentally studied the pulsating film cooling effectiveness and concluded that pulsating jet at high frequency will improve the film cooling performance by preventing cooling jet from rolling up. While the results for pulsating flow at low frequency will be opposite. Ekkad[10] studied the influence of pulsating jet duty cycle on heat transfer based on a model with leading edge film cooling. It is concluded that the duty cycle leads to lower blowing momentum and fine spreading of the cooling air on the wall. To sum up, there still has no uniform conclusion about whether jet pulsation enhances film cooling performance or not.

For the numerical research, the traditional CFD method based on Reynolds time average (RANS) model cannot capture the complex flow structures like small vortices[11]. The direct numerical simulation (DNS) resolves all the time and length scales and thus is computationally expensive. As compromise model, the large eddy simulation (LES) only resolves the larger time and length scales and uses a subgrid-scale model for the smaller eddies instead[12]. In addition, it is a great challenge to analyze the large amounts of spatiotemporal data emerging from DNS and LES[13]. The dynamic modal decomposition (DMD) approach originally proposed by Schmid[14] is a tool of dealing with the spatiotemporal data by decomposing time-resolved data into modes, with each mode having a single characteristic frequency. It is a data-driven algorithm[15] and combines favorable aspects of both the POD and the discrete Fourier transform[16] by extracts dynamic information like spatiotemporal coherent structure from unsteady experimental or numerical flow field[17]. Therefore, the DMD is proper for studying the pulsating effect on film cooling. Kalghatgi[18] made experiments and LES simulation of the plate film cooling, and then discussed the origin and evolution of the vortex structure by DMD modal analysis of the velocity and temperature field. It is found that the low-frequency hairpin vortex has important influence on the wall temperature, while the high-frequency K-H mode has a great impact on the mixing region near the film cooling holes. Zhao [19] made direct numerical simulation of a low momentum laminar jet discharged into a laminar channel crossflow through a circular orifice. The computational results are analyzed via model order reduction techniques: the Proper Orthogonal Decomposition (POD) and Dynamic Mode Decomposition (DMD). It is shown that the DMD approach with the ranking with respect to the amplitudes averaged over time is the most efficient technique for the problem in study.

To sum up, the effect of jet pulsation on cooling efficiency has not been unified concluded, and results from many literature are even contradictory. In the present paper, the FLIR thermal infrared thermal camera is used to measure the pulsating film cooling efficiency. To analyze the effect of the pulsating jet on film cooling performance, simulations by LES is conducted and the instantaneous flow field is analyzed. In addition, the DMD dynamic mode analysis of the velocity and temperature field is made to explain the relationship of pulsating jet and cooling effectiveness.

2 Experimental facilities

The experimental platform for film cooling was designed and built to measure the cooling efficiency of plane film cooling. The schematic diagram of the experimental system is shown in Fig.1, which is mainly composed of the mainstream and jet gas paths. The mainstream is produced by an air compressor, and heated by an electric heater, then flows through the rectifier section and test section, equipped with some valves, data measurement and acquisition systems as well. The rectification section includes the contraction and expansion section with a cellular network rectifier in the middle. To reduce the heat loss, the whole test section is wrapped with insulation layer, as shown in Fig.2.

The cooling jet is supplied by a small pump and flows through a collecting chamber before flowing out the film hole. The collecting chamber can produce pulsating jet by a vibrating diaphragm loudspeaker at the bottom. The signal generators and amplifiers provide sinusoidal signal with different frequency and amplitude to drive the loudspeaker vibrating.

The test section is a rectangular channel with a cross section of 50×80mm^2 and a length of 500 mm. The film cooling hole is located on the mid-line of the plate, with 20mm away from the inlet, and a diameter of 13mm. The jet from the film hole is inclined and 30 deg angled to the mainstream. The adiabatic temperature of the cooling surface is measured by IR camera, which is fixed directly above the test section. A total of 16 thermocouples were arranged on the midline of the plate surface to measure the airflow temperature immediately adjacent to the wall. These T-type thermocouples have a diameter of 0.65 mm, and are inserted from the bottom of the cooling surface, as seen in Fig.3

The inlet velocity of the mainstream is u_∞=5 m/s without any fluctuation. The turbulence intensity of the freestream is 12%. The inlet temperature of the mainstream is set to be T_∞=330K. The initial temperature of coolant is T_c=290K. The average velocity of the jet coolant sets the average blowing ratio of pulsating jet coolant is $M=\rho_c U_c/\rho_\infty U_\infty$=0.65, 1.0 and 1.5. The characteristic frequency of the velocity for the pulsating jet is f and its nondimensionalized value is $St=f\cdot D/U_c$=0, 0.1, 0.2 and 0.3.

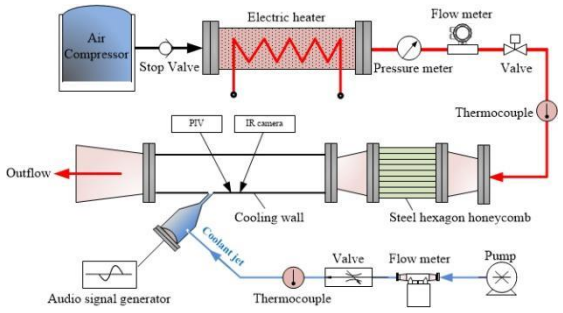

Fig.1 Sketch of Experimental system

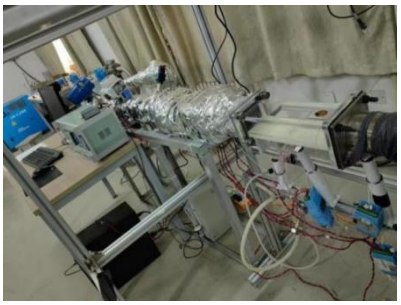

Fig.2 Photo of experimental system wrapped with insulation cotton

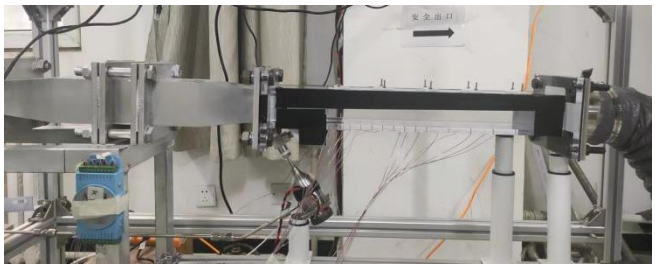

Fig.3 Photo of the test section

3. Numerical Method

3.1. Numerical Schemes and Computation Setup

The computational domain is selected to be the same with the experimental test section. It a rectangular channel with a cross section of 3.85*D*×6.15*D* and a length of 36.92*D*. The cylindrical film cooling hole is located at the center-line of the cooling wall with 6.92*D* away from the inlet of mainstream, and a diameter of *D*=13mm. The jet from the film hole is inclined and 30 deg angled to the mainstream. The details of the geometry can be seen in Fig.4.

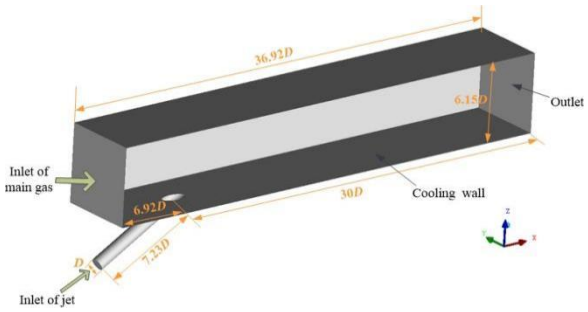

Fig.4 Computational domain

The structured hexahedral mesh and its enlarged view are shown in Fig.5. The O-type grids near film hole is refined to meets the requirements of the low Reynolds number turbulence model. The distance of the first grid point off the surface, measured in wall units (y^+), is less than unity. Three sets of grids 3,000,000, 6,000,000 and 8,000,000 are calculated and compared to achieve grid independence. And the final size of the mesh is 6×10^6 cells.

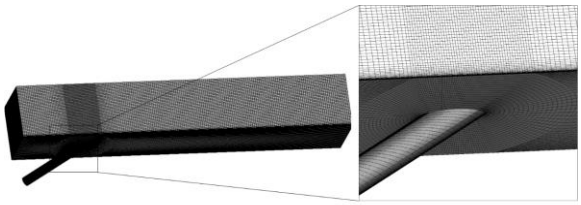

Fig.5 The grids and enlarged view

The flow boundary conditions are consistent with the experimental operating condition. The inlet temperature of the mainstream is 330K. The inlet velocity of the mainstream is 5m/s, and has a turbulence boundary layer with a thickness of δ/D=1.0 adopting the 1/7 exponential distribution law.

The inlet temperature of the jet is 290K. The injecting jet coolant is sinusoidal pulsated with an velocity expression of:

$$u_c = U_c + \sin(2\pi ft) \tag{1}$$

where U_c is the average velocity of the jet coolant. The cooling wall is non-slip adiabatic wall. The left and right surface of the passage domain are periodic wall boundary conditions. The inlet of the passage is total pressure inlet boundary condition and the outlet is pressure outlet boundary condition, respectively. The wall adapting local eddy viscosity (WALE) model is selected. The pressure-velocity coupling adopts the semi-implicit algorithm of the pressure-coupled equations. The simulation was run for 5,000 time steps and the time step is set to be 4.8×10^{-5}s.

The numerical prediction is performed on ANSYS FLUENT to solve the transient Navier-Stokes equation. In LES, the density-weighted method proposed by Faver is used to filter the compressible Navier-Storks equation, as follows:

$$\frac{\partial \bar{\rho}}{\partial t} + \frac{\partial}{\partial x_j}(\bar{\rho}\tilde{u}_j) = 0 \tag{2}$$

$$\frac{\partial \bar{\rho}\tilde{u}_j}{\partial t} + \frac{\partial}{\partial x_j}(\bar{\rho}\tilde{u}_i\tilde{u}_j) = -\frac{\partial \tilde{p}}{\partial x_i} + \delta_{ij} - \tilde{\tau}_{ij} - \tau_{u_i u_j}) = 0 \tag{3}$$

$$\frac{\partial \bar{\rho}\tilde{h}}{\partial t} + \frac{\partial}{\partial x_j}(\bar{\rho}\tilde{u}_j\tilde{h} + \bar{\rho}a\frac{\partial \tilde{h}}{\partial x_j} - \tau_{u_j h}) = 0 \tag{4}$$

$$\bar{\rho} = \frac{p_0}{\tilde{RT}} \tag{5}$$

where ρ, u, μ, p, τ_{ij}, λ and h are density, velocity, dynamic viscosity, pressure, subgrid-scale stress, thermal conductivity and sensible enthalpy, respectively. The subgrid-scale turbulence models in Ansys Fluent employ the Boussinesq hypothesis as in the RANS models, computing subgrid-scale turbulent stresses from

$$\tilde{\tau}_{ij} - \frac{1}{3}\tau_{kk}\delta_{ij} = -2\mu_t \bar{S}_{ij} \tag{6}$$

where μ_t is the subgrid-scale turbulent viscosity. The isotropic part of the subgrid-scale stresses is not modeled, but added to the filtered static pressure term.is the rate-of-strain tensor for the resolved scale defined by

$$\bar{S}_{ij} = \frac{1}{2}(\frac{\partial \bar{u}_i}{\partial x_j} + \frac{\partial \bar{u}_j}{\partial x_i}) \tag{7}$$

In the WALE model, the eddy viscosity is modeled by

$$\mu_t = \rho L_s^2 \frac{(S_{ij}^d S_{ij}^d)^{3/2}}{(\bar{S}_{ij}\bar{S}_{ij})^{5/2} + (S_{ij}^d S_{ij}^d)^{5/4}} \tag{8}$$

Where $L_s$and S_{ij}^d in the WALE model are defined, respectively, as

$$L_s = \min(\kappa d, C_w V^{1/3}) \tag{9}$$

$$S_{ij}^{d}=\frac{1}{2}(\bar{g}_{ij}^{2}+\bar{g}_{ji}^{2})-\frac{1}{3}\delta_{ij}\bar{g}_{kk}^{2},\bar{g}_{ij}^{2}=\frac{\partial\bar{u}_i}{\partial x_j} \tag{10}$$

where κ is the von Kármán constant. The published value for the WALE constant, C_w, is 0.5; however, intensive validation during a European Union research project involving the original model developers has shown consistently superior results in Ansys Fluent with C_w= 0.325, and so it is this value that is used as the default setting.

3.2. Numerical Verification

To verify the numerical results, the LES numerical results are compared with the experiment of Sultan[8]. Figure 6 shows the flow direction velocity u_x in the normal direction at x=3.5D, St=0, x=3.5D, St=0.3, x=5.5D, St=0, and x=5.5D, St=0.3. It can be seen that the LES calculated velocity agrees well with the experimental value, with an error of about 5%. The centerline adiabatic film cooling effectiveness at M=0.65are compared and shown in Fig.7. The statistical analysis of validation is also made bu adding the results of Sultan[8]. The experimental results in the present study agrees well with the numerical results and a little higher than the results of Sultan after x/D>8.

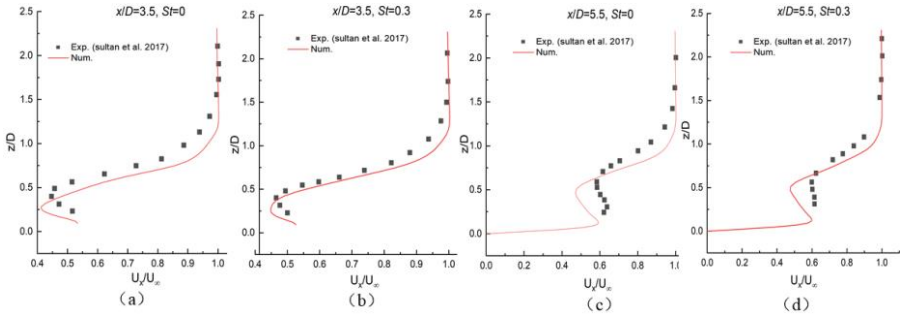

Fig.6 The flow velocity at x/D=3.5 downstream of the hole

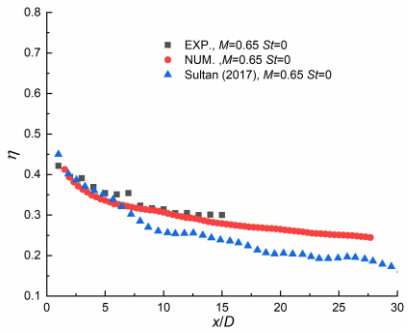

Fig.7 Centerline film cooling effectiveness the along the flow direction

4. Flow and Heat transfer Analysis

The film cooling performance of the pulsating cooling jet can be judged by the parameter adiabatic film cooling effectiveness η of the wall, which is defined as:

$$\eta=\frac{T_{aw}-T_{\infty}}{T_{c}-T_{\infty}} \tag{11}$$

where T_{aw} is the adiabatic surface temperature.

4.1. Effect of blowing ratio and pulsating frequency on film cooling effectiveness

The measured cooling effectiveness by IR at three different blowing ratio M=0.65, 1.0 and 1.5 are shown in Fig.8(a), (b) and (c), respectively. It can be seen that the cooling effectiveness is much higher around the film hole and decreases along the flow direction. The spots shown in the contour are the mounting holes for the T-type thermcouples arranged on the midline of the plate surface. At steady film cooling (St=0), the cooling effectiveness decreases with the increase of blowing ratio, which is because the cooling air is lifted by the kidney-shaped vortex. With the increase of the blowing ratio, the kidney-shaped vortex is enhanced, and the jet downstream gradually deviates from the wall. The cooling efficiency near the film hole is the highest. The shape of its distribution is coincides with the horseshoe vortex formed by the transverse jet.

At low blowing ratio (M=0.65), shown in Fig.8(a), the cooling efficiency of the pulsating jet is significantly lower than the steady-state jet. At blowing ratio of 1.0 and 1.5, the cooling efficiency of the low frequency pulsating jet (St=0.2) is a little higher than the steady state jet near the film hole, indicating that the low frequency pulsation under the high blowing ratio can improve the coverage of the cooling air near the film hole. This because that at a medium St=0.2, the pulsating jets with various velocity will mix and collide at the outlet of the jet and produces smaller vortex, consequently. The collision between the pulsating jets and mainstream will lead to reduction of flow momentum in the flow direction but increase of flow momentum in the spanwise direction. At high pulsating frequency (St=0.3), the cooling effectiveness is obviously declined. At high St=0.5, This collision occurs at the outlet of the film hole and the secondary vortex is much smaller, and causes a significant reduction of the flow momentum.

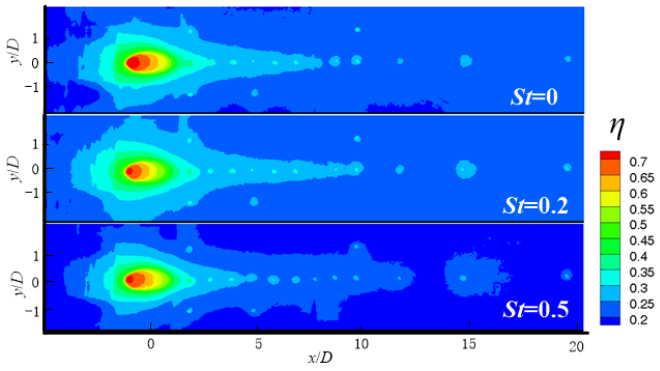

(a) M=0.65

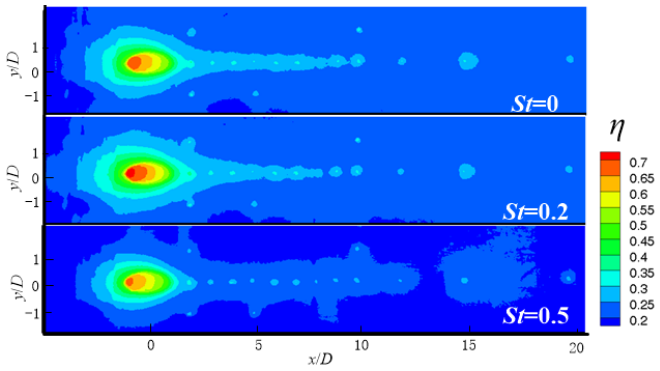

(b) M=1.0

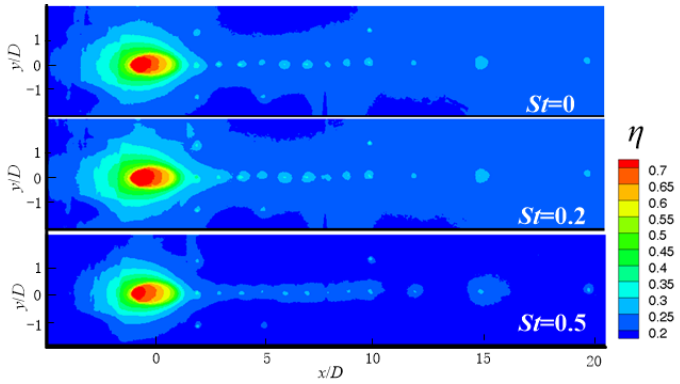

(c) M=1.5

Fig.8 Measured cooling effectiveness at different blowing ratio

4.2. The Flow fields structure

To analyze the film cooling effectiveness of the pulsating jet, the instantaneous coherent structures indicated by Q criterion near the wall for the steady jet at M=0.65 is shown in Fig.9. The sketch of cooling air injecting into mainstream can be seen in Fig.9(a). Since the injection angle of jet is 30°, the cooling air attaches to the wall closely and shows waves on the top edge. The principal vortex structure is hairpin vortex whose heads developing from shear layer vortex at the interface of the jet and mainstream, and two legs developing from the counter rotating vortex pairs (CVP). Therefore, the head and leg of hairpin vortex promote the mixing of jet air with mainstream by lifting cooling air flow away from the wall. Horseshoe vortices can be observed around the film holes, which will gradually develop into small hairpin vortices on the right and left side.

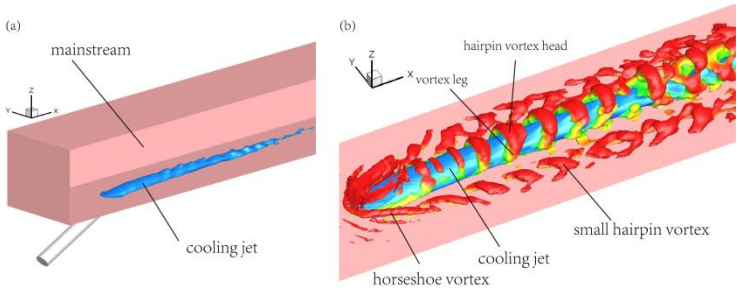

Fig.9 The instantaneous vortex structure

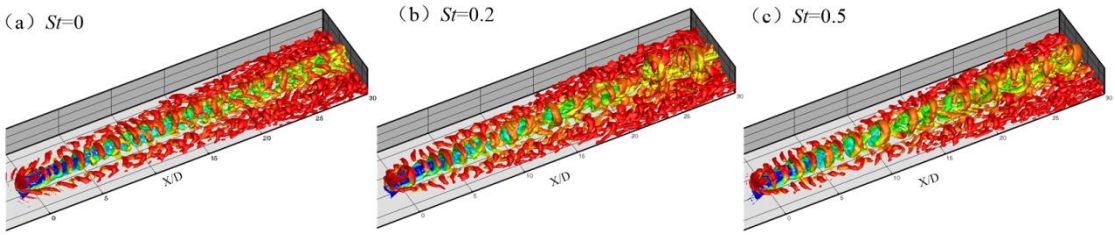

Fig.10 The instantaneous vortex structure

The whole coherent structures identified by Q criterion at t=1/4T for M=0.65, St=0, 0.2, and 0.5 are shown in Fig.10. The mixing process of jet and mainstream can be divided into four stages: fusing, falling, developing and breaking stage. It can be seen that, compared with the steady state (St=0), the

quantity of small and broken vortices downstream the jet hole for the pulsating jet is much larger, indicating that the pulsating jet promotes the hairpin vortex breaking into smaller vortex and spread in the spanwise direction at the broken stage (x/D>15).

5 Modal Analysis of flow

The LES calculated results of transient flow field and the temperature field are analyzed by DMD to study the effect of the pulsating jet on film cooling effectiveness.

5.1. Description of algorithm

The dynamic mode decomposition (DMD) technique is performed by extracting the hydrodynamic modes from time-resolved data, and each mode has a characteristic frequency of oscillation and growth/decay rate. The dominant eigenvalues and modes are extracted through mathematical transformation of data matrix from experiments or simulations[20]. The details of the procedure of DMD is referred to Kutz [13].

5.2. DMD using velocity data

In this part, the general exact DMD algorithm is used for dynamic modal decomposition of the calculation velocity results. The snapshot time interval is 0.00048s. A total of 50 snapshots are used as the data source of modal decomposition under each working condition.

The modal energy distribution over the entire DMD domain for M=0.65, St=0, 0.2 and 0.5 is shown in Fig.11(a), (b), (c) and (d), respectively. Five modes with top energy level are marked with mode A, B, C, D and E (arranged by the flow energy level from high to low). The mode A with a characteristic frequency of 0 Hz represents the nonoscillating mean flow component.

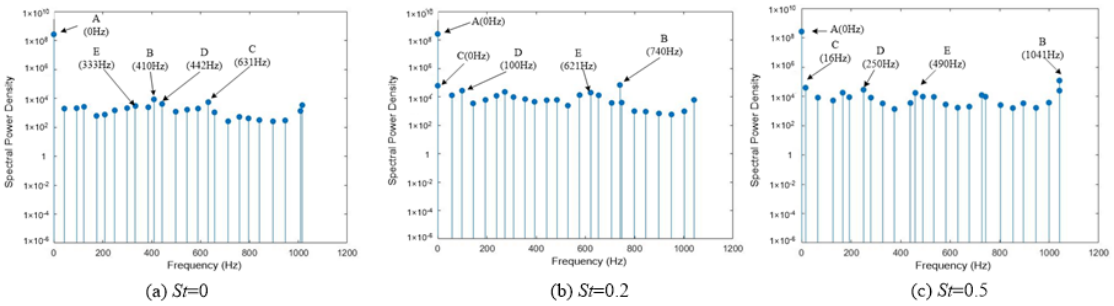

(a) St=0 (b) St=0.2 (c) St=0.5

Fig.11 DMD energy spectrum for the Mid-section velocity

The normalization flow velocity component to x direction at the mid-cross section for the five modes are shown in Fig.12. The decomposition velocity in mode A is a steady-state component. For steady jet shown in Fig.12(a), in mode B there are obvious periodic hairpin vortex with corresponding frequency of about 410Hz. The frequency of mode C is 631Hz, in which there are smaller secondary vortex structures. The periodic arranged vortex structure of mode D is a shear layer vortex formed by the velocity gradient at the bottom of the jet, corresponding to a frequency of 440Hz. The velocity component of mode E is the shedding vortex of the horseshoe vortex, with a frequency of 333Hz.

For St=0.2 shown in Fig.12(b), The mode B is the secondary vortex of the hairpin vortex, corresponding to a frequency of 740Hz. Mode C is the velocity drift mode. The velocity component of

mode D is periodic vortex pairs and has a frequency of 100Hz, equal to the corresponding frequency of sinusoidal pulsating jet at *St*=0.2. Therefore, the large vortices in mode D are caused by the pulsating jet. For *St*=0.5, mode B of is also secondary vortex structures. In Mode D, the velocity component is reverse vortex pair with periodic arrangement and has a frequency of 250Hz, equal to the pulsating frequency. The mode E represents the hairpin vortex structure, and has frequency of 490Hz, which is twice the pulsating frequency.

Through DMD, high energy flow structures can be extracted from the velocity data. The generating frequency of Haripin vortex is about 410-490Hz. The frequency of high energy secondary vortex broken from hairpin is about 700Hz. Then the small vortice broken from horseshoe vortex has a frequency of 330Hz. In addition, the pulsating jet will produce big and periodic vortex.

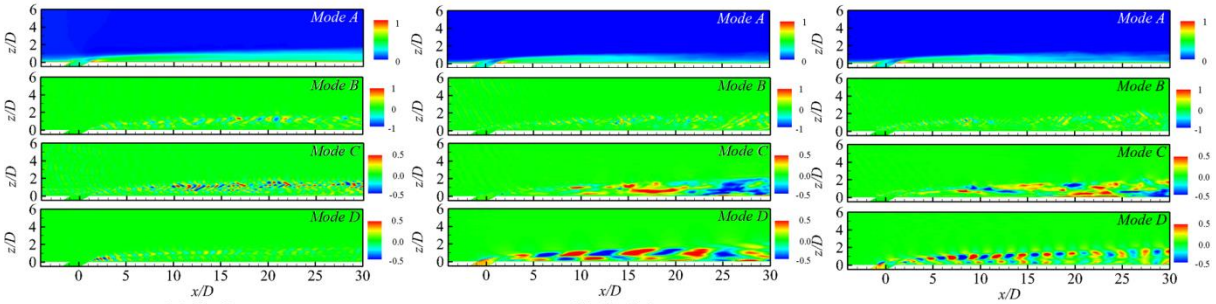

(a) *St*=0 (b) *St*=0.2 (c) *St*=0.5

Fig.12 Mid-section velocity mode distribution

5.3. DMD using temperature data

In order to determine the dominant modes contributing to surface heat transfer, modes of wall temperature fluctuation are extracted. Frequency of these extracted modes is listed in Fig.13, on which Five top level energy modes are marked as A, B, C, D, and E (arranged by the energy level from high to low). The high energy mode basically concentrated in the low frequency region, indicating that higher frequency flow has less impact on the temperature fluctuations. In addition, the frequency of high-energy mode for temperature is totally different from the high energy velocity mode, which means that the variation of the velocity vector is not synchronous with the temperature scalar.

Figure 14 gives the contour of temperature fluctuations components of mode A, B, C, D and E for *M*=0.65, *St*=0, 0.2 and 0.5. Mode A represents the mean temperature component, corresponding to a frequency of 0Hz. For steady jet *St*=0, the temperature fluctuation mainly occurs near the film hole, while the temperature fluctuation for the pulsating jet is severe downstream of the hole. For *St*=0.2, there are regular periodic vortices in mode B with corresponding frequency is 100Hz. So there periodic vortices are caused by jet sinusoidal pulsation. What is more, the shape of the temperature fluctuation is the symmetric vortex leg shape, indicating that the wall temperature distribution is affected by vortex leg structure. The broken of hairpin vortex in the downstream reduces the temperature fluctuation. The temperature fluctuations in modes C and E are caused by low-frequency vortex structure. The mode D is temperature drift mode. For *St*=0.5, the frequency of mode E is 250Hz, which is the same with the pulsating frequency of cooling jet, and the temperature fluctuation occurs around the film hole.

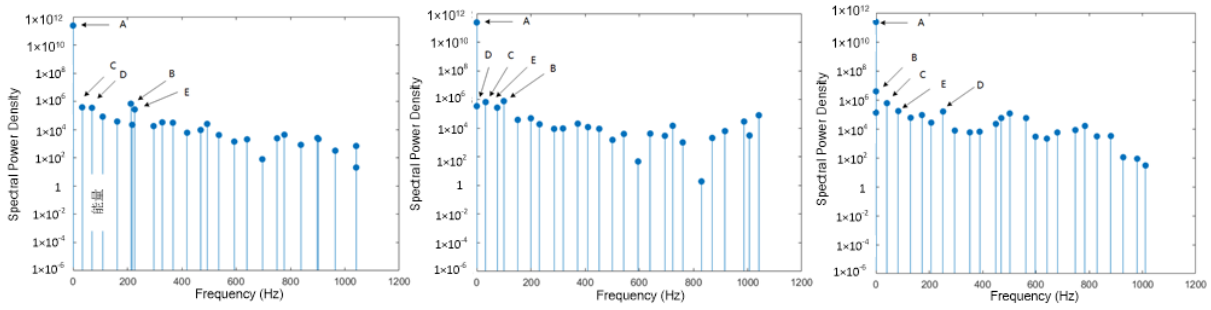

(a) *St*=0 (b) *St*=0.2 (c) *St*=0.5

Fig.13 DMD energy spectrum of wall surface temperature

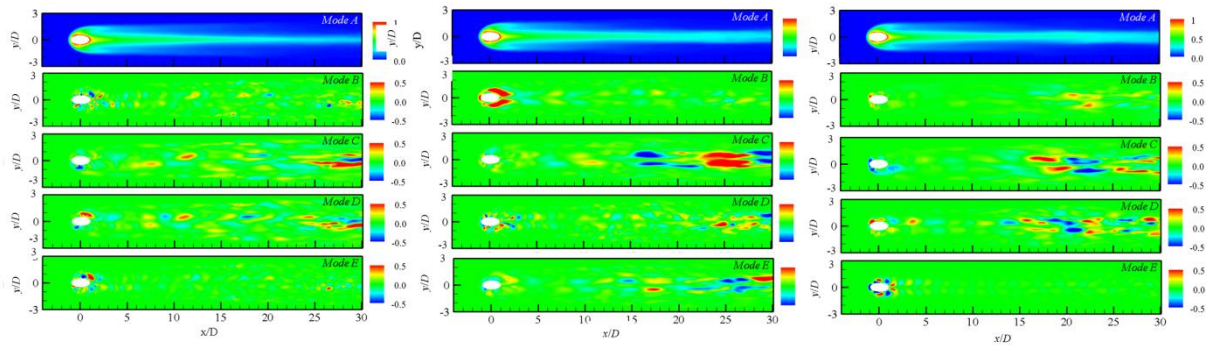

(a) *St*=0 (b) *St*=0.2 (c) *St*=0.5

Fig.14 Surface temperature mode of mode A, B, C, D and E

6. Conclusion

The flow and heat transfer of pulsating film cooling was calculated by LES. Then the flow field structure was analyzed by using the dynamic mode decomposition method (DMD). The main conclusions are as follows:

(1) The cooling effectiveness of steady film cooling (*St*=0) decreases with the increase of blowing ratio. At low blowing ratio (*M*=0.65), the cooling efficiency of the pulsating jet is significantly lower than the steady-state jet. At the blowing ratio of 1.0 and 1.5, the cooling efficiency of the low frequency pulsating jet (*St*=0.2) is a little higher than the steady state jet, indicating that the low frequency pulsation under the high blowing ratio can improve the coverage of the cooling air. At high pulsating frequency (*St*=0.5), the cooling effectiveness is obviously declined.

(2) By the modal analysis of the velocity and temperature data, it is found that the jet pulsation produces many secondary vortex structures, which promotes the spread of cooling jet and increases cooling effectiveness. The low frequency vortex structure leads to the temperature fluctuations, while the high frequency vortex structure affects the average temperature component in the steady state.

Acknowledgement

This work was supported by the Open Research Fund of the State Key Laboratory of Mechanical Manufacturing System Engineering, Xi'an Jiaotong University (sklms2021015), Project of natural science research in Shanxi province (No.202203021211122), and National natural sciences fund youth fund project (No.52305459).

References

[1] Goldstein R J . Film Cooling, *Advances in Heat Transfer*, (1971), 7, pp.321-379.

[2]Ahn, Joon. Large Eddy Simulation of Film Cooling: A Review, *Energies*, 15(2022),23, pp.8876.
[3]Oliver T.A., Bogard D.G., Moser R.D., Large eddy simulation of compressible, shaped-hole film cooling, *International Journal of Heat and Mass Transfer*, 140(2019), pp.498-517.
[4]Yuefeng Li, Huazhao Xu, Jianhua Wang, Junqiang Zhu, Yun Chen, Large Eddy Simulation of trenched cylindrical film hole with backward compound angles, *International Journal of Thermal Sciences*, 184(2023), pp.107910.
[5]Hosseini, S.M., Zirak S., Zargarabadi, M.R., Pulsed film cooling on a complete turbine blade: steady, sinusoidal and square injections, *J. Therm Anal Calorim*, 148(2023), pp.9761-9783.
[6]F. Muldoon, S. Acharya, DNS study of pulsed film cooling for enhanced cooling effectiveness, *Int. J. Heat Mass Transf*, 52(2009), pp.3118-3127.
[7]Bons, J.P., Rivir, J.B., Mac Arthur, C.D., et al., The Effect of Unsteadiness on Film Cooling Effectiveness, Wright Laboratory, Report No. WL-TR-96-2096, 1995.
[8]Sultan, Qaiser, Lalizel, et al. Influence of Coolant Jet Pulsation on the Convective Film Cooling of an Adiabatic Wall, *Journal of heat transfer: Transactions of the ASME*, 139(2017), pp.022201.
[9]Coulthard S.M., Volino R.J., Flack K.A., Effect of Jet Pulsing on Film Cooling-Part I: Effectiveness and Flow-Field Temperature Results, *Journal of Turbomachinery*, 2006.
[10]Ekkad S.V.,Ou S., Rivir R.B., Effect of Jet Pulsation and Duty Cycle on Film Cooling From a Single Jet on a Leading Edge Model, *Journal of Turbomachinery*, 128(2006), 3, pp.564-571.
[11]Foroutan, Hosein, Yavuzkurt, et al., Numerical Simulations of the Near-Field Region of Film Cooling Jets Under High Free Stream Turbulence: Application of RANS and Hybrid URANS/Large Eddy Simulation Models, *Journal of heat transfer: Transactions of the ASME*, 137(2015), 1.
[12] Dupuy, Dorian, et al. Boundary-condition models of film-cooling holes for large-eddy simulation of turbine vanes, *International Journal of Heat and Mass Transfer*, 166(2021), 2, pp.120763.
[13]Hamzehloo, ArashLusher, et.al., On the performance of WENO/TENO schemes to resolve turbulence in DNS/LES of high-speed compressible flows, *International Journal for Numerical Methods in Fluids*, 93(2021), 1.
[14]Schmidt, P.J., Dynamic Mode Decomposition of Numerical and Experimental Data, *J. Fluid. Mech.*, 656(2010), pp.5-28.
[15]Kutz J.N., Nathan J., Brunton S.L., et al., *Dynamic mode decomposition: data-driven modeling of complex systems*, Soc. Ind. Appl. Math., 2016.
[16]Rowley C.W., Igor M., Shervin B., et al. Spectral analysis of nonlinear flows, *J. Fluid Mech.*, (2009).
[17]Kou J.Q, Zhang W.W. Dynamic mode decomposition and its applications in fluid dynamics, *Acta Aerodynamica Sinica*, 36(2018), 2, pp.163-179.
[18]Kalghatgi P., Acharya S., Modal Analysis of Inclined Film Cooling Jet Flow, *J. Turbomach.*, 136(2014), 8, pp.081007.
[19]Wu, Zhao, et al., Proper orthogonal decomposition and dynamic mode decomposition of jet in channel crossflow, *Nuclear Engineering and Design*, 344(2019), 4, pp.54-68.
[20]Schmid P.J., Li L., Juniper M.P., et al., Applications of the dynamic mode decomposition, *Theoretical & Computational Fluid Dynamics*, 25(2011), 4, pp.249-259.

Submitted: 25.09.2023.
Revised: 01.12.2023.
Accepted: 12.12.2023.